Supporting Information Appendix

Role of vascular normalization in benefit from metronomic chemotherapy: Insights from a mathematical model

Fotios Mpekris, James W. Baish, Triantafyllos Stylianopoulos, Rakesh K. Jain

Description of the mathematical model

The mathematical model accounts for the growth of a spherical tumor with initial diameter 500 μm surrounded by normal tissue. Tumor growth is modeled based on principles of continuum mechanics and specifically, on the multiplicative decomposition of the deformation gradient tensor (**F**), which describes the kinematics of the tumor. The kinematics of the tumor are decomposed into two components, the growth component ($\mathbf{F}_g$) that accounts for the growth of the tumor and the elastic component ($\mathbf{F}_e$) that accounts for mechanical interactions of the tumor with the surrounding normal tissue (1, 2),

$$\mathbf{F} = \mathbf{F}_e \mathbf{F}_g, \tag{1}$$

The growth component is set to be homogenous and isotropic (3-5)

$$\mathbf{F}_g = \lambda_g \mathbf{I}, \tag{2}$$

where λ_g is the growth stretch ratio, which describes the growth of cancer cells and cancer stem cells (proliferation minus apoptosis). The elastic component $\mathbf{F}_e$ of the deformation gradient tensor is determined from Eq. (1) as

$$\mathbf{F}_e = \mathbf{F}\ \mathbf{F}_{\boldsymbol{g}}^{-1}. \tag{3}$$

Calculation of growth stretch ratio λ_g

We calculated the growth rate of the tumor taking into account the oxygen concentration as well as non-stem cancer cell (CC), stem-cell-like cancer cell (CSC) and induced cancer cell (ICC) proliferation (3, 4, 6-8). In particular, we used the expression

$$\frac{d\lambda_g}{dt} = \frac{1}{3}\left(\frac{T}{T_{tot}} S_T^c + \frac{C_{sc}}{T_{tot}} S_{C_{sc}}^c + \frac{I}{T_{tot}} S_I^c\right)\lambda_g, \tag{4}$$

where T is the CC population, C_{sc} is the CSC population, I is the ICC population, T_{tot} is the total density of cells given by the sum of the three populations, and S_T^C, S_{Csc}^C and S_I^C are the proliferation/degradation rates of CCs, CSCs and ICCs, respectively. The proliferation/degradation rates are taken to be a function of oxygen concentration and the fraction of CCs, CSCs and ICCs, killed by chemotherapy or by immune cells (Eq. 5).

Immune response to tumor growth

For the immune system, three types of immune cells are considered, the natural killer (NK) cells the $CD8^+$ T-cells and the regulatory T cells (Treg) (9-11). The system of equations accounts for the recruitment rates of the immune cells, their inactivation by cancer cells, the inhibitory role of Treg cells as well as their death rate and interaction with cancer cells.

The equations that describe the conservation of cancer and immune cells are given below:

$$\begin{aligned}
\frac{\partial T}{\partial t} &= GS_{ftr}T - cNT - D + p_{CT}C_{sc} + p_{IT}I - \left(p_{TC} + p_{TI}\right)T \\
\frac{\partial C_{sc}}{\partial t} &= \alpha_{\mathrm{csc}}GS_{ftr_{\mathrm{csc}}}C_{sc} - c_{\mathrm{csc}}NC_{sc} - D_{\mathrm{csc}} + p_{TC}T + p_{IC}I - \left(p_{CT} + p_{CI}\right)C_{sc} \\
\frac{\partial I}{\partial t} &= \alpha_I GS_{ftr_I}I - c_I NI - D_I + p_{TI}T + p_{CI}C_{sc} - \left(p_{IT} + p_{IC}\right)I \\
\frac{\partial N}{\partial t} &= \sigma_{nk} - f_{NK}N + \frac{g_{NK}T^2}{h+T^2}N - p_{im}NT - \lambda_{reg}T_{reg}N \\
\frac{\partial L}{\partial t} &= -m_{T8}L + \frac{j_{T8}D^2}{k_{im}+D^2}L - qLT + rNT - \lambda_{reg}T_{reg}L \\
\frac{\partial T_{reg}}{\partial t} &= g_{reg}T_{reg} - m_{reg}T_{reg}
\end{aligned} \tag{5}$$

where N is the density of NK cells, L is density of tumor-specific $CD8^+$ T-cells and T_{reg} is the density of the Treg cells. In the equations above all cell densities are a function of position and time, and the migration of different cell types relative to the tissue is neglected. G describes the proliferation of CCs, CSCs and ICCs as a function of oxygen and S_f is an expression that accounts for the fraction of cells surviving chemotherapy. The proliferation of CSCs and ICCs is corrected by multiplying the expression for CCs by α_{csc} and α_I, respectively according to experimental evidence (8, 12), c and D are the fractions of tumor cells killed by NK and $CD8^+$ T-cells, respectively, f_{NK}, m_{T8} and m_{reg} are death rates of NK cells, $CD8^+$ T-cells and Treg cells

respectively, g_{NK}, j_{T8} and g_{reg} are recruitment rates of immune cells, p_{im} and q are inactivation rates of immune cells by CCs, σ_{nk} is a constant source of NK cells, r is the rate at which tumor-specific $CD8^+$ T cells are stimulated to be produced as a result of tumor cells killed by NK cells and λ_{reg} is the inhibition term of NK cells and $CD8^+$ T cells from Treg cells. The rates of transfer of cancer cells from a type i to a type j are described by p_{ij} and their values were determined in (8) . Owing to a lack of studies that relate directly oxygen levels to activity of NK or CD8-T cells that our model incorporates, we used values from the range given by de Pillis et al. Under complete hypoxic conditions we used the lowest value for the activity of NK cells and $CD8^+$ T cells reported in de Pillis et al. (9) which increased linearly to the highest value for normal oxygen conditions. The values of f_{NK} and m_{T8} are modified to depend on oxygen levels. According to experimental data (13), a 40 times decrease in oxygen concentration (from 20% to 0.5%) doubled the apoptotic rate of immune cells. Furthermore, the recruitment rates g_{NK}, j_{T8} and g_{reg} of NK cells, $CD8^+$ T-cells and Treg cells respectively, were modified to account for the effect of chemotherapy. According to previous studies (14) chemotherapy can decrease the number of Treg cells by a factor of four but low dose chemotherapy has no effect on the population of NK cells and $CD8^+$ T-cells. At high doses of chemotherapy, however, the population of NK and $CD8^+$ cells decreases by a factor of two. The range of values of the parameters of Eq. 5 are given in de Pillis et. al., based on preclinical and clinical data and from other pertinent studies (Table S1). The above equations are rendered dimensionless by dividing the number of cells per finite element node by the initial number of cancer cells, $T_0=5\times10^2$ cells. The initial population of cancer cells was taken to be: 98% CCs, 1% CSCs and 1% ICCs (15).

The parameter D denotes the fractional cell kill of tumor cells by $CD8^+$ T-cells and given by equation:

$$D = d_{im}\frac{\left(\frac{L}{T}\right)^{\lambda_{im}}}{s+\left(\frac{L}{T}\right)^{\lambda_{im}}}T\,, \tag{6}$$

where d_{im} is the saturation level of fractional tumor cell kill by $CD8^+$ T-cells, s is steepness coefficient of the tumor-$CD8^+$ T-cells competition term and λ_{im} the exponent of fractional cell kill by $CD8^+$ T-cells.

The experimentally observed dependence of the volumetric growth rate on the local oxygen concentration is described by G and has the form (16, 17)

$$G = \frac{k_1 c_{ox}}{k_2 + c_{ox}}, \tag{7}$$

where k_1 and k_2 are growth rate parameters and c_{ox} is the oxygen concentration. To account for the effect of drug delivery on growth, the surviving fraction of cells S_{ftr} is included in Eq. (5), so that in the absence of drugs S_{ftr} equals unity. The fraction of surviving cells with respect to drug concentration has been previously measured experimentally for doxorubicin (18), and the results were fitted to an exponential expression as a function of the internalized chemotherapy concentration c_{int}, i.e.,

$$S_f = \exp(-\omega c_{int}), \tag{8}$$

where ω is a fitting parameter defined in (19) for doxorubicin. According to this equation, if we ignore immune cells and assume that CCs, CSCs and ICCs, are killed by chemotherapy, the terms S_T^c, S_{Csc}^C S_I^C in Equation 12 become zero and thus, the growth stretch ratio in Equation 4 gets a constant value. One would expect that the growth stretch ratio will decrease when CCs, CSCs and ICCs are killed, instead of taking a constant value. To account for this, Equation 8 was modified in the form:

$$S_{ftr} = 2*(\exp(-\omega c_{int})-0.5) \tag{9}$$

Due to the fact that CSCs are chemoresistant, we fit the equation to experimental data (20) to find the fitting parameter ω for this case (S_{ftrcsc}). Additionally, even though different drugs might be incorporated into the model, in its current form the model does not distinguish between drugs assuming that their potency (i.e., parameter ω) is identical.

For the proliferation rates of CSCs and ICCs, α_{csc} and α_I, respectively we assume that for normal oxygen levels they are the same as the proliferation of CCs. In hypoxic conditions, for their growth rates we assume that they increase inversely proportional to the oxygen concentration so that as oxygen concentration approaches zero, the proliferation rates are twice as much as the rate at normal oxygen (12). For the parameters c_{csc}, D_{csc}, c_I, and D_I that describe the killing potential of immune cells on CSCs and ICCs, we assume that they are more resistant in

interactions with immune cells. According to experimental data (21), the cytotoxicity of $CD8^+$ T-cells against CSCs is taken to be 7-fold lower than that of CCs. As a result, the parameters that describe the death of CSCs due to immune cells are assumed to be the same as for the CCs but multiplied with a factor of 0.14. For the ICCs, we assume that the dependence on drug delivery, oxygen concentration and immune response is the same as for the CSCs.

Biphasic formulation of the tumor's mechanical behavior

The conservation of the tumor's solid and fluid phase is given by the following mass balance equations (3, 7):

$$\frac{\partial \Phi^c}{\partial t} + \nabla \cdot (\mathbf{v}^s \Phi^c) = \frac{T}{T_{tot}} S_T^c + \frac{C_{sc}}{T_{tot}} S_{\mathrm{Csc}}^c + \frac{I}{T_{tot}} S_I^c , \tag{10}$$

$$\frac{\partial \Phi^f}{\partial t} + \nabla \cdot (\mathbf{v}^f \Phi^f) = Q , \tag{11}$$

where Φ^c and Φ^f are the volume fractions of the solid and fluid phases, respectively, and $\mathbf{v}^s$, $\mathbf{v}^f$ are the corresponding velocities. The creation/degradation of the solid phase, S_T^c, S_{Csc}^C and S_I^C was expressed in accordance to Equation (5) and Ref. (3):

$$\begin{aligned} S_T^c &= GS_{ftr} T - cNT - D + p_{CT} C_{sc} + p_{IT} I - \left(p_{TC} + p_{TI} \right) T \\ S_{Csc}^c &= \alpha_{\mathrm{csc}} GS_{ftr_{\mathrm{csc}}} C_{sc} - c_{\mathrm{csc}} NC_{sc} - D_{\mathrm{csc}} + p_{TC} T + p_{IC} I - \left(p_{CT} + p_{CI} \right) C_{sc} \\ S_I^c &= \alpha_I GS_{ftr_I} I - c_I NI - D_I + p_{TI} T + p_{CI} C_{sc} - \left(p_{IT} + p_{IC} \right) I \end{aligned} \tag{12}$$

The term Q in Eq. (11) denotes the fluid flux entering from the blood vessels into the tumor or the surrounding normal tissue minus the fluid flux exiting through lymphatic vessels, and is expressed as (5):

$$Q = L_p S_v (p_v - p_i) - L_{pl} S_{vl} (p_i - p_l) , \tag{13}$$

where L_p, S_v and p_v are the hydraulic conductivity, vascular density and vascular pressure, respectively, L_{pl}, S_{vl} and p_l are the corresponding quantities for lymphatic vessels, and p_i is the interstitial fluid pressure. Due to conservation of matter in the tissue, the volume fraction of the fluid phase was evaluated as

$$\Phi^f = 1 - \Phi^c . \tag{14}$$

Furthermore, the mass balance reads

$$\nabla \cdot \left(\Phi^c \mathbf{v}^s + \Phi^f \mathbf{v}^f \right) = Q + \frac{T}{T_{tot}} S_T^c + \frac{C_{sc}}{T_{tot}} S_{\mathrm{Csc}}^c + \frac{I}{T_{tot}} S_I^c , \tag{15}$$

where the fluid velocity $\mathbf{v}^f$ is given by Darcy's law

$$\mathbf{v}^f = \frac{-k_{th} \nabla p_i}{\Phi^f} + \mathbf{v}^s , \tag{16}$$

with k_{th} the hydraulic conductivity of the interstitial space.

According to the biphasic theory for soft tissues (22), the total stress tensor $\boldsymbol{\sigma}_{tot}$ is the sum of the fluid phase stress tensor $\boldsymbol{\sigma}^f = -p_i\mathbf{I}$ and the solid phase stress tensor $\boldsymbol{\sigma}^s$. As a result, the stress balance is written as:

$$\nabla \cdot \boldsymbol{\sigma}_{tot} = \mathbf{0} \Rightarrow \nabla \cdot (\boldsymbol{\sigma}^s - p_i \mathbf{I}) = \mathbf{0} , \tag{17}$$

where the Cauchy stress tensor of the solid phase $\boldsymbol{\sigma}^s$ is given by (23):

$$\boldsymbol{\sigma}^s = J_e^{-1} \mathbf{F}_e \frac{\partial W}{\partial \mathbf{F}_e^T} , \tag{18}$$

The tumor mechanical behavior was modeled to be incompressible and neo-Hookean with strain energy density given by (24-27):

$$W = \frac{\mu(-3 + II_1)}{2} - p\left(-1 + J_e + \frac{p}{2k} \right), \tag{19}$$

where μ and k are the shear and bulk modulus of the material, respectively, J_e is the determinant of the elastic deformation gradient tensor $\mathbf{F}_e$, $II_1 = I_1 J_e^{-2/3}$ where $I_1 = \mathrm{tr}\mathbf{C}_e$ is the first invariant of the elastic Cauchy-Green deformation tensor $\mathbf{C}_e = \mathbf{F}_e^{\mathrm{T}} \mathbf{F}_e$, and p is a penalty variable introduced for near incompressible materials. The surrounding normal tissue was assumed to be compressible and neo-Hookean with a Poisson ratio of 0.2. Values for all parameters above are provided in Table S1.

Equations (1-3) and (10-19) provide the general framework of the biomechanical tumor growth model and are solved to simulate the growth of the tumor within a normal/host tissue. Solution of these equations is used for the calculation of the interstitial fluid pressure, the fluid velocity and the stresses that are developed owing to mechanical interactions of the tumor with the host tissue.

Interstitial fluid pressure and fluid velocity are used in the drag transport equations (Eq. 23, 24), whereas mechanical interactions between the tumor and the host tissue affect how much the tumor will growth. Equations (4-9) describe the balance law of the different cell types into the tumor to calculate the growth stretch ratio, λ_g, which determines how fast the tumor will grow. The growth stretch ratio is employed by the general framework through Equations (2, 3 and 18).

Vascular surface density

To quantify the vascular density we assume that it is affected by the decrease in the vessel diameter caused by increased number of cancer cells (28) and by the permeability of the tumor vessel wall (29). To incorporate the effect of the former, we considered the vascular density as the vascular surface area *S* per unit volume, with *S* given by:

$$S = \pi d L_{vw} N, \tag{20}$$

where d, L_{vw} and N are the diameter, length and number of vessels, respectively. Assuming that the number of cancer cells does not affect the number or length of vessels, but only their diameter, the change in vascular density due to vessel compression is expressed as:

$$S_V = (d/d_0)\, S_{V0}, \tag{21}$$

where S_{V0} is the vascular density of the host tissue, $S_{V0} = 70\ \text{cm}^{-1}$. Fitting experimental data from histological sections (28, 30) to a mathematical equation, an expression for degree of vessel compression (i.e., *d/do*) as a function of cancer cell density can be estimated (Fig. S14). For low cancer cell density, d/d_o=1 and the vascular density is equal to the reference vascular density S_{vo} given in Figure S5C.

For the effect of vascular permeability on the functional vessel density, our previous research has shown that a decrease in the vessel wall pore size from 400nm (baseline value) to 150 nm or less causes a two-fold increase in the number of functional vessels and that the dependence in this range of vessel wall pore sizes is linear (29).

Oxygen Concentration

The rate of change of oxygen in tissues depends on its transport through convection and diffusion, minus the amount of oxygen consumed by cells, plus the amount that enters the tissue from the blood vessels (3, 4), i.e.,

$$\frac{\partial c_{ox}}{\partial t} + \nabla \cdot \left(c_{ox} \mathbf{v}^f \right) = D_{ox} \nabla^2 c_{ox} - \frac{A_{ox} c_{ox}}{c_{ox} + k_{ox}} \Phi^C + P_{er} S_V \left(C_{iox} - c_{ox} \right), \tag{22}$$

where c_{ox} is the oxygen concentration, D_{ox} is the diffusion coefficient of oxygen in the interstitial space, A_{ox} and k_{ox} are oxygen uptake parameters, P_{er} is the vascular permeability of oxygen that describes diffusion across the tumor vessel wall and C_{iox} is the oxygen concentration in the vessels.

Drug transport

We assumed that the chemotherapeutic agent exists in three distinct states: free to travel in the interstitial space (c_f), bound to cancer cells (c_b), and internalized by cells (31). Hence, drug transport in the interstitial space is expressed as (32):

$$\begin{aligned} \frac{\partial c_f}{\partial t} + \nabla \cdot \left(c_f \mathbf{v}^f \right) &= D_f \nabla^2 c_f + Q_{sta} - \frac{k_{on} c_e c_f}{\Phi} + k_{off} c_b, \\ \frac{\partial c_b}{\partial t} + \nabla \cdot \left(c_b \mathbf{v}^s \right) &= \frac{k_{on} c_e c_f}{\Phi} - k_{off} c_b - k_{int} c_{int}, \\ \frac{\partial c_{int}}{\partial t} + \nabla \cdot \left(c_{int} \mathbf{v}^s \right) &= k_{int} c_b, \end{aligned} \tag{23}$$

where D_f is the diffusion coefficient of the drug in the tumor interstitial space, c_e is the concentration of cell surface receptors, k_{on}, k_{off} and k_{int} are the association (binding), dissociation and internalization rate constants of the drug with the cells, respectively, and Φ is the volume fraction of tumor accessible to the drug. The term Q_{sta} on the right hand side of Eq. (23) denotes the transport of the drug across the tumor vessel wall and is given by Starling's approximation as (32):

$$Q_{sta} = P_{er} S_V (C_{iv} - c_f) + L_p S_V (P_V - p_i)(1 - \sigma_f) c_f \tag{24}$$

where L_p is the hydraulic conductivity of the vessel wall, $C_{iv} = \exp(-(t-t_0)/k_d)$ is the vascular concentration of the drug, describing a bolus injection, with t_0 the time of drug injection and k_d the blood circulation decay, and σ_f is the reflection coefficient. The hydraulic conductivity was calculated from the expression (33):

$$L_p = \frac{\gamma r_0^2}{8\eta L_{vw}}, \tag{25}$$

where γ is the fraction of vessel wall surface area occupied by pores, r_0 is the pore radius, η is the viscosity of water at 310K, and L_{vw} is the thickness of the vessel wall.

The vascular permeability P_{er} and the reflection coefficient σ_f were calculated from the equations:

$$P_{er} = \frac{\gamma H D_0}{L_{vw}} \tag{26}$$

$$\sigma_f = 1 - W \tag{27}$$

respectively, where H and W describe hydrodynamic and electrostatic interactions and D_0 is the diffusion coefficient of a particle in free solution at 310K, given by the Stokes-Einstein relationship

$$D_0 = \frac{K_b T_{emp}}{6\pi\eta r_s}, \tag{28}$$

where K_b is the Boltzmann constant, T_{emp} is temperature and r_s the radius of the diffusing particle. Ignoring electrostatic interactions, H and W are reduced to (33):

$$H = \frac{6\pi F}{K_t}, \tag{29}$$

$$W = \frac{F(2-F)K_s}{2K_t}, \tag{30}$$

where F is the partition coefficient (33):

$$F = (1-\lambda)^2, \tag{31}$$

and λ is the ratio of the drug size to the vessel wall pore size. The coefficients K_s and K_t in Eqs. (29) and (30) are determined by:

$$\begin{pmatrix} K_t \\ K_s \end{pmatrix} = \frac{9}{4}\pi^2\sqrt{2}\left(1-\lambda\right)^{-5/2}\left[1+\sum_{n=1}^{2}\begin{pmatrix} a_n \\ b_n \end{pmatrix}\left(1-\lambda\right)^n\right]+\sum_{n=0}^{4}\begin{pmatrix} a_{n+3} \\ b_{n+3} \end{pmatrix}\lambda^n . \quad (32)$$

In the case of oxygen, γ and H in Eq. (26) were set equal to unity assuming that oxygen diffuses through any point of the vessel wall and its transport is not hindered by hydrodynamic interactions; D_0 for oxygen was taken to be the same as the diffusion coefficient in the tissue (D_{ox} in Table S1), i.e.:

$$P_{erox} = \frac{D_0}{L_{vw}} . \quad (33)$$

Solution strategy

The model consists of a spherical tumor domain embedded at the center of a cubic host domain two orders of magnitude larger to avoid any boundary effects on the growth of the tumor; due to symmetry, only one eighth of the system was considered. We simulated a murine tumor that grows within a period of 30 days based on published experimental protocols (34-36). To this end, Equations (1)-(33) were solved simultaneously using the commercial finite element software COMSOL Multiphysics (COMSOL, Inc., Burlington, MA, USA). Values for the model parameters are provided in Supplementary Table 1. The boundary conditions for the continuity of the stress and displacement fields, as well as the concentration of the oxygen and the drug at the interface between the tumor and the normal tissue, were applied automatically by the software, the remaining boundary conditions are shown in Fig. S15.

Table S1 Parameter values used in the model

Parameter	Description	Value	Reference
μ	shear modulus	5.00 kPa for host tissue; 10.40 kPa for tumor	(37-39)
k	bulk modulus	6.67 kPa for host tissue; 10.40×10^{7} kPa for tumor	(37-39)
k_{th}	hydraulic conductivity	6.5×10^{-10} $m^2\cdot Pa^{-1}\cdot day^{-1}$	(39)
C_{iox}	initial oxygen concentration	0.2 $mol\cdot m^{-3}$	(4,15)
D_{ox}	oxygen diffusion coefficient	1.55×10^{-4} $m^2\cdot day^{-1}$	(4)
A_{ox}	oxygen uptake	2,200 $mol\cdot m^{-3}\cdot day^{-1}$	(4, 17)
k_{ox}	oxygen uptake	0.00464 $mol\cdot m^{-3}$	(4, 17)
k_1	growth rate parameter	3,500 day^{-1}	---
k_2	growth rate parameter	0.0083 $mol\cdot m^{-3}$	(17)
c_e	receptor concentration	0.01 $mol\cdot m^{-3}$	(40, 41)
Φ	volume fraction of tumor accessible to drug	0.3	(40, 41)
k_{on}	binding rate	1.296×10^{6} $m^3\cdot mol^{-1}\cdot day^{-1}$	(40, 41)
k_{off}	dissociation rate	691.2 day^{-1}	(40, 41)
k_{int}	internalization rate	3.7 day^{-1}	(40, 41)
D_f	drug diffusion coefficient	8.64×10^{-6} $m^2\cdot day^{-1}$	(42)
ω	cancer cell survival constant	0.6603 m^3/mol	(19)
ω_{csc}	stem-cell-like cell survival constant	0.0272 m^3/mol	(19, 20)
ω_{I}	induced cancer cell	0.0272 m^3/mol	---

	survival constant		
a_{csc}	stem-cell-like cell growth multiplier	range **: 1-2 [-]	(11)
a_I	induced cancer cell growth multiplier	range **: 1-2 [-]	---
k_d	blood circulation decay	0.417 day^{-1}	(43)
L_{vw}	vessel wall thickness	5×10^{-6} m	(5)
η	water viscosity at 310K	7×10^{-4} Pa·s	(5)
T_{abs}	absolute temperature	310K	---
γ	fraction of vessel wall surface area occupied by pores	1×10^{-5} [-]	(43)
c	fractional tumor cell kill by NK cells	range *: 3.23×10^{-7} - 3.23×10^{-6} $cell^{-1}\cdot day^{-1}$	(44)
d_{im}	fractional tumor cell kill by $CD8^+$ T-cells	range *: 1.43 – 7.15 day^{-1}	(44)
λ_{im}	exponent of fractional cell kill by $CD8^+$ T-cells	1.36 [-]	(44)
s	steepness coefficient of the tumor-$CD8^+$ T-cells competition term	2.73 [-]	(44)
σ_{nk}	constant source of NK cells	1.3×10^4 cells·day^{-1}	(44)
f_{Nk}	death rate of NK cells	range **: 0.0412 - 0.0814 day^{-1}	(44)
m_{T8}	death rate of $CD8^+$ T-cells	range **: 0.02 - 0.04 day^{-1}	(44)
m_{reg}	death rate of regulatory T-cells	0.02 day^{-1}	(10)

g_{NK}	recruitment rate of NK cells	initial***: 0.025 day^{-1}	(44)
j_{T8}	recruitment rate of $CD8^+$ T-cells	initial***: 0.0375 day^{-1}	(44)
g_{reg}	recruitment rate of regulatory T-cells	initial***: 0.0375 day^{-1}	(10)
h	steepness coefficient of NK cell recruitment curve	2.02×10^{7} $cell^{2}$	(44)
p_{im}	inactivation rate of NK cells	1×10^{-7} $cell^{-1}\cdot day^{-1}$	(44)
k_{im}	steepness coefficient of $CD8^+$ T-cells recruitment curve	2.02×10^{7} $cell^{2}$	(44)
q	inactivation rate of $CD8^+$ T-cells	3.42×10^{-10} $cell^{-1}\cdot day^{-1}$	(44)
r	stimulation rate of $CD8^+$ T-cells	1.1×10^{-7} $cell^{-1}\cdot day^{-1}$	(44)
λ_{reg}	inhibition term of NK cells and $CD8^+$ T-cells from T-reg cells	100 $cell^{-1}\cdot day^{-1}$	(10)
p_{TC}	rate of dedifferentiation from cancer cells to stem-like-cell cancer cells	0.55 day^{-1} prior treatment; 0 day^{-1} after application of chemotherapy	(8)
p_{CT}	rate of transition from stem-like-cell cancer cells to cancer cells	1 day^{-1} prior treatment; 0.96 day^{-1} after application of chemotherapy	(8)
p_{CI}	rate of transition from stem-like-cell cancer	0.58 day^{-1} prior treatment; 0 day^{-1} after application of	(8)

	cells to induced cancer cells	chemotherapy	
p_{IC}	rate of transition from induced cancer cells to stem-like-cell cancer cells	0.96 day^{-1} prior treatment; 0.38 day^{-1} after application of chemotherapy	(8)
p_{TI}	rate of transition from cancer cells to induced cancer cells	0.21 day^{-1} prior treatment; 1 day^{-1} after application of chemotherapy	(8)
p_{IT}	rate of transition from induced cancer cells to cancer cells	1 day^{-1} prior treatment; 0.98 day^{-1} after application of chemotherapy	(8)

*: linear increase from minimum to maximum value depending on oxygen levels

**: linear decrease from maximum to minimum value depending on oxygen levels

***: initial value in the absence of drug.

Table S2 Value of parameter k_1 used for fitting the model to experimental data

Experimental study	k_1
Doloff et al.(45)	1,950 day^{-1}
Cham et. al.(35)	800 day^{-1} (PaCa8) 1,100 day^{-1} (PaCa13)
Yapp et. al. (46)	2,400 day^{-1} (PaCa8) 2,600 day^{-1} (PaCa13)

Figure S1 Effect of TSP-1 variation on (**A**) functional vascular density, (i.e., S_v in Supplementary Eq. 21), (**B**) tissue oxygenation, (**C**) drug concentration taken up by all types of cancer cells, (**D**) NK cell, (**E**) CD8+ T cell and (**F**) Treg cell population defined as number of cells per computational node normalized with initial cancer cells concentration. Drug concentration was normalized with the vascular concentration. The values of the model parameters were calculated in the middle distance between the tumor center and periphery.

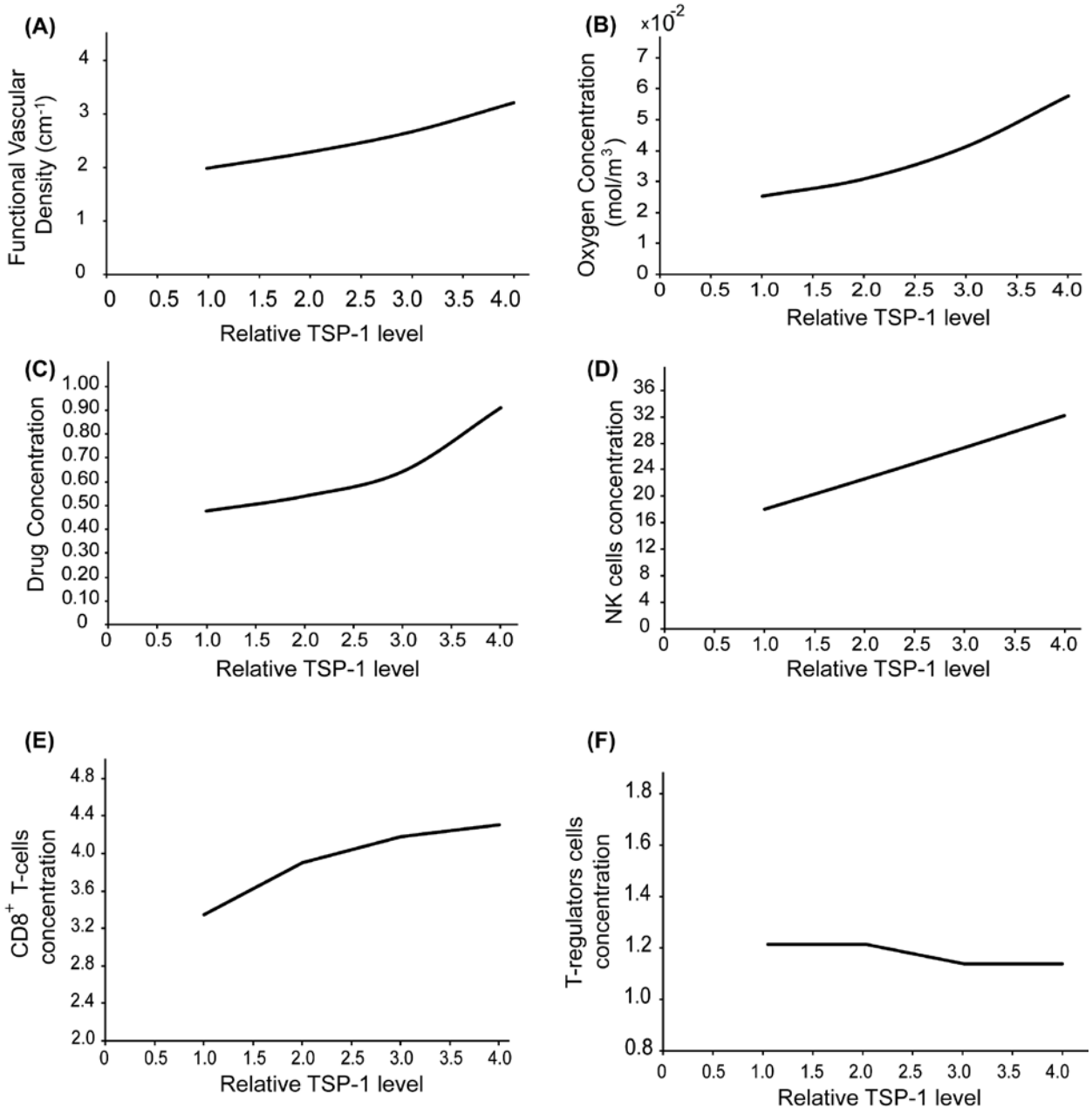

Figure S2 Effect of TSP-1 variation on (**A**) cancer cell, (**B**) stem-cell-like cancer cell and (C) induced cancer cell population - defined as number of cells per computational node normalized with the initial cancer cells concentration and on (**D**) final tumor volume at the end of the simulation. The values of the model parameters were calculated in the middle distance between the tumor center and periphery.

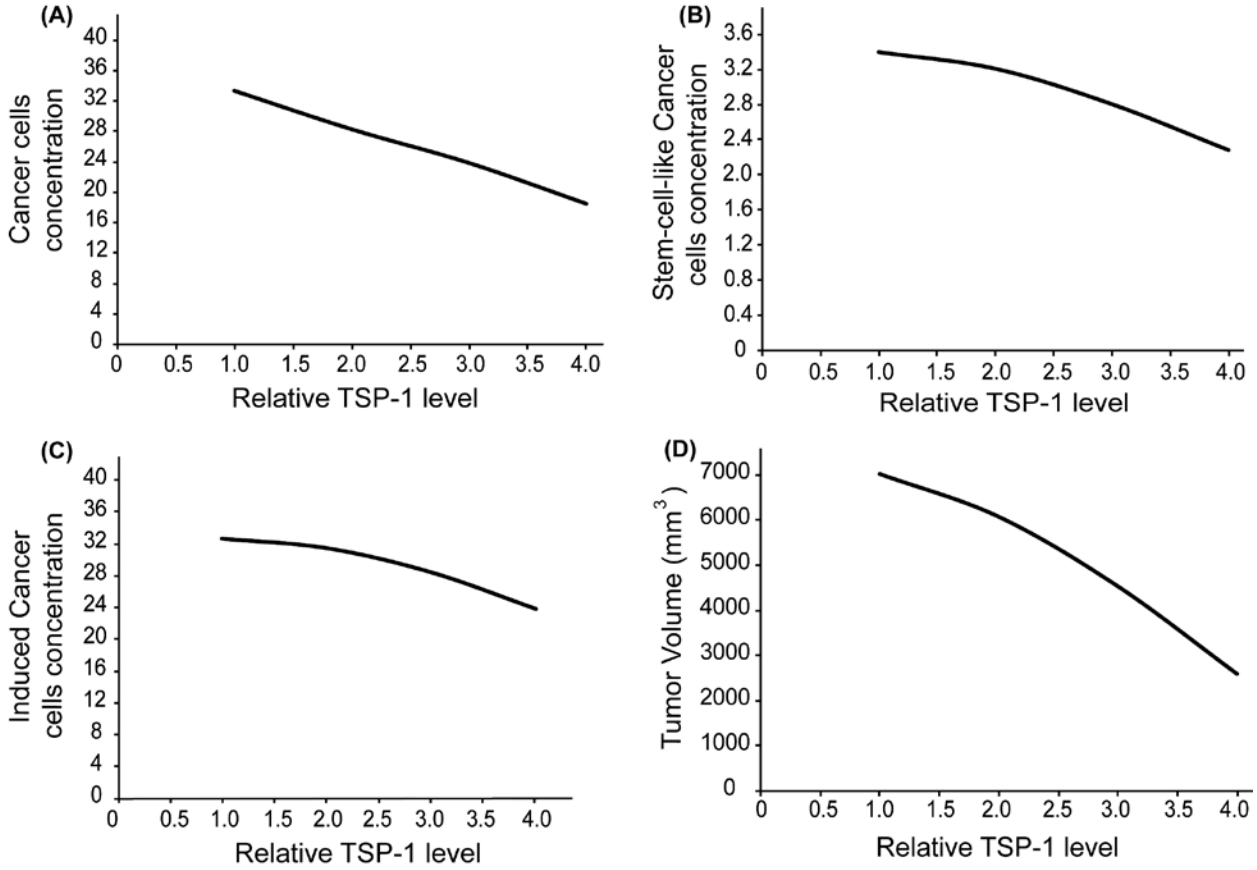

Figure S3 Spatial distribution of various quantities. Increase in TSP-1 levels leading to increase of (A) oxygen levels, (B) drug concentration (dimensionless with respect to the concentration in the vessels), (C) NK cells and (D) $CD8^+$ T-cells concentration and decrease of (E) cancer cells (F) stem-cell-like cancer cells and (G) induced cancer cells concentration. Cell concentration is defined as number of cells per computational node normalized with the initial cancer cells concentration. The total number of computational nodes for the tumor domain is 135.

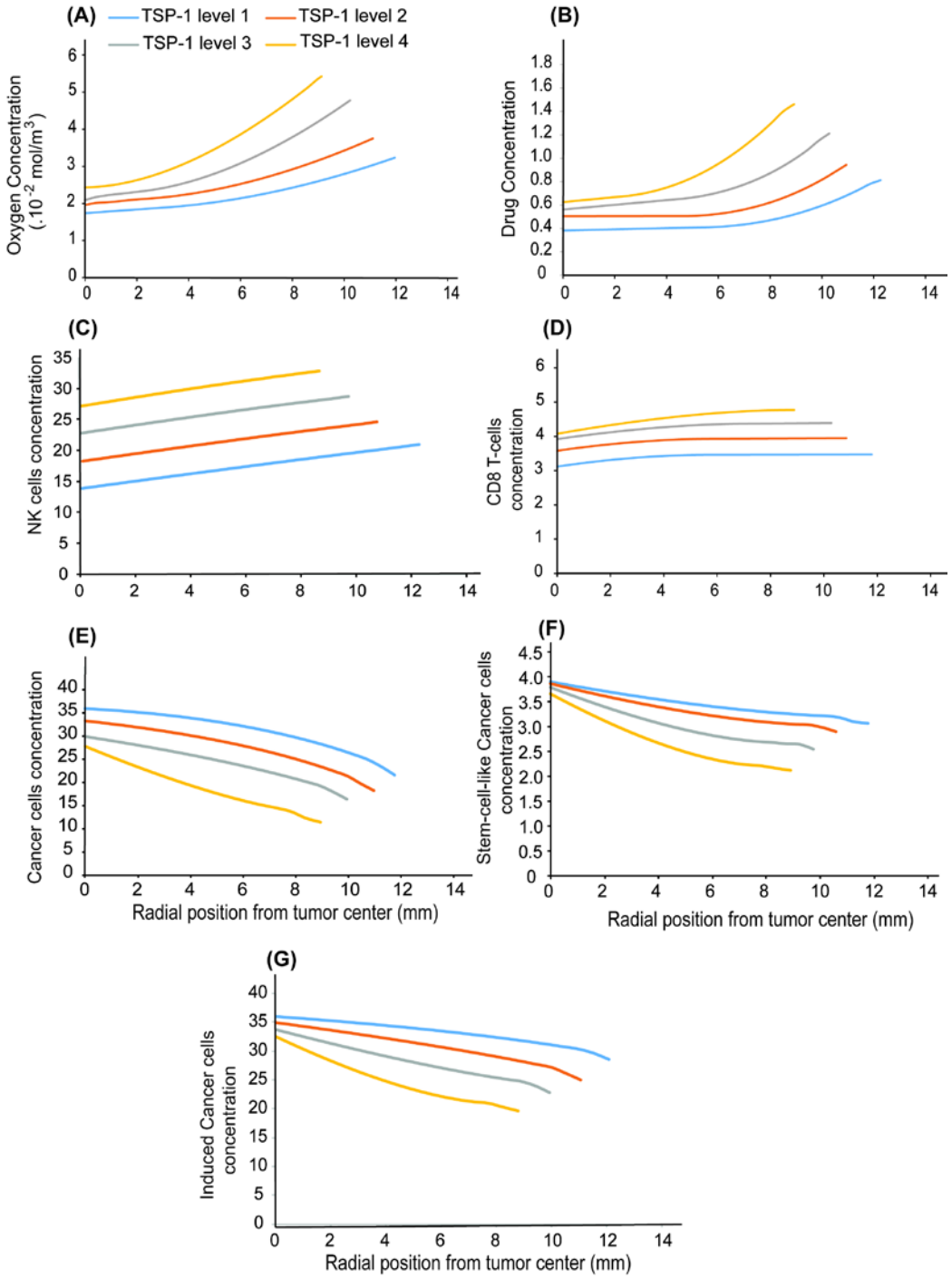

Figure S4 Proportion of populations (A-C) and total number of cell population (D-F; logarithmic scale) of all cell types considered in the model without chemotherapy (**A, D**) and with chemotherapy using two different levels of TSP-1; (**B, E**) TSP-1 level 1 and (**C, F**) TSP-1 level 4. Model results for the population of the three cancer cell types are in agreement with previous studies (8). Increase of TSP-1 levels results in an increase in the population of induced cancer cells (ICCs) due to the fact that are more resistant to increased drug levels compared to cancer cells (CCs). Furthermore, the initial increase in the population of NK cells is also observed in Ref. (9) where the equations of the immune cells were first used and validated.

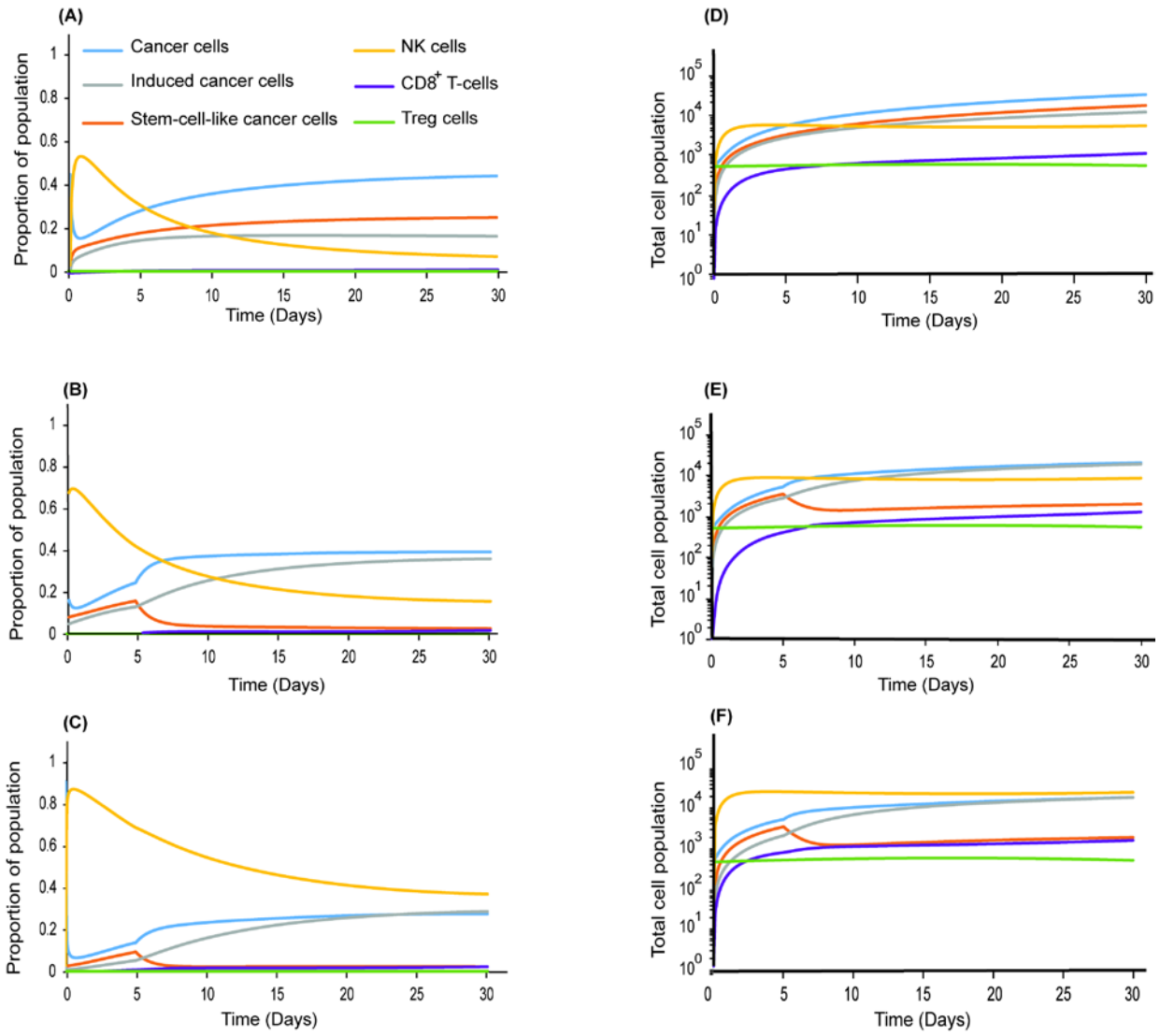

Figure S5 Model assumptions for TSP-1 levels and TSP-1 induced vessel normalization. (**A**) A sigmoidal function was employed to describe the relationship of relative increase of TSP-1 with the dose schedule (47). Dose of unity corresponds to the MTD protocol, while lower doses to different metronomic therapy protocols. (**B**) Dependence of vessel wall pore size (47) (vascular permeability) on TSP-1 relative increase with respect to the TSP-1 amount of MTD. (**C**) Dependence of initial functional vessel density (i.e., S_{vo} in Supplementary Eq. 21) on the relative TSP-1 increase with respect to the TSP-1 amount of MTD (29).

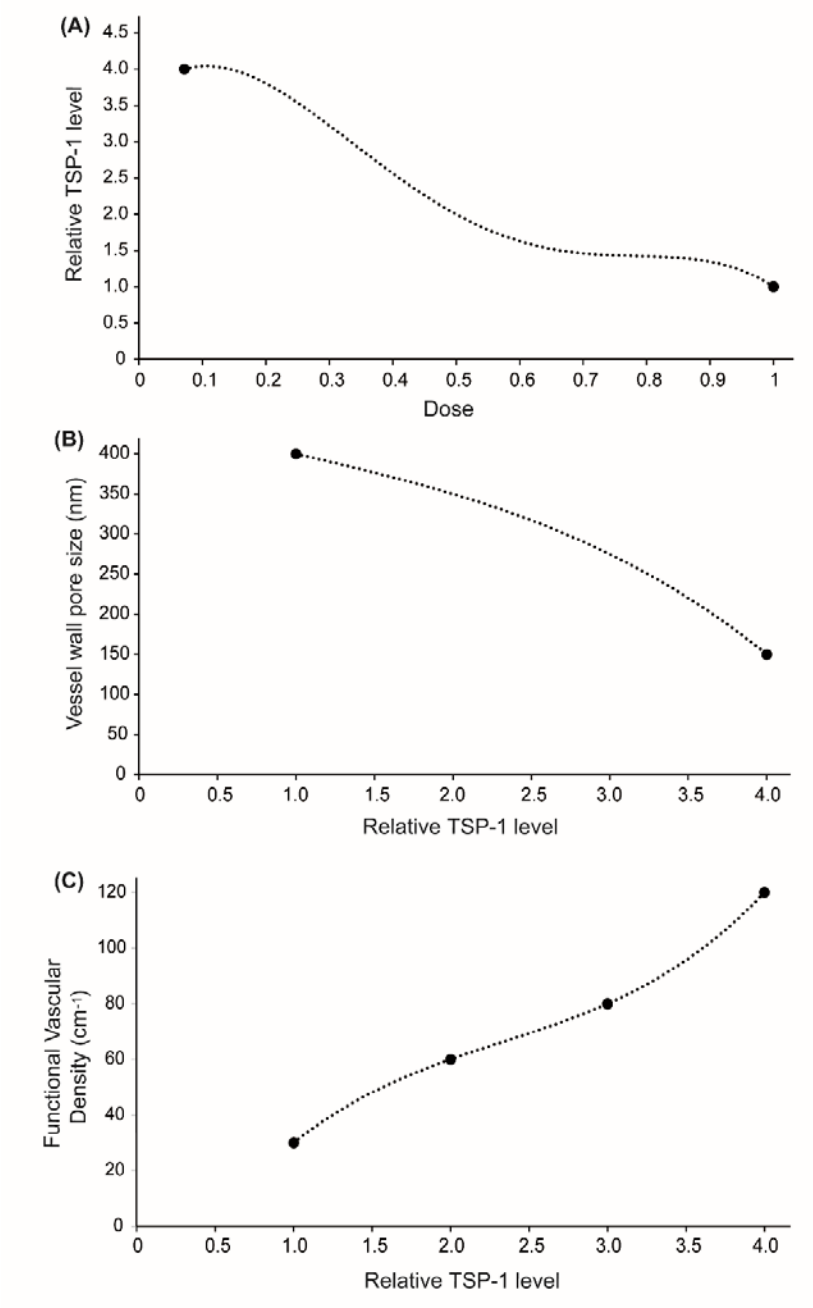

Figure S6 Phase diagram for the effect of dose scheduling and tumor relapse/cell recovery on (**A**) $CD8^+$ T-cells and (**B**) Treg concentration. Low dose chemotherapy increases levels of $CD8^+$ T-cells and decreases slightly levels of Treg cells. Relative values of metronomic therapy with respect to the corresponding values of the MTD protocol are presented. The values of the model parameters presented in the figure were calculated in the middle distance between the tumor center and periphery.

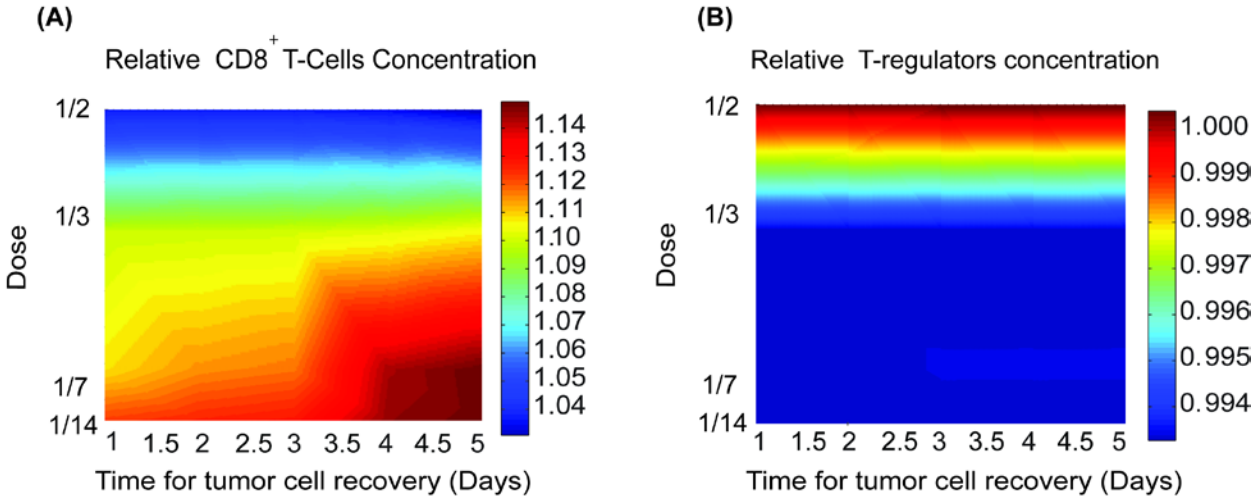

Figure S7 Total cancer cells population as a function of time for the MTD protocol (solid line) and metronomic protocol (dashed line) - the lowest dose employed - for three different times for tumor relapse (1, 2 and 4 days). The decrease and recovery of cancer cells following drug administration with MTD is shown, which is absent for the metronomic protocol. Cell concentration is normalized with the initial cancer cells concentration.

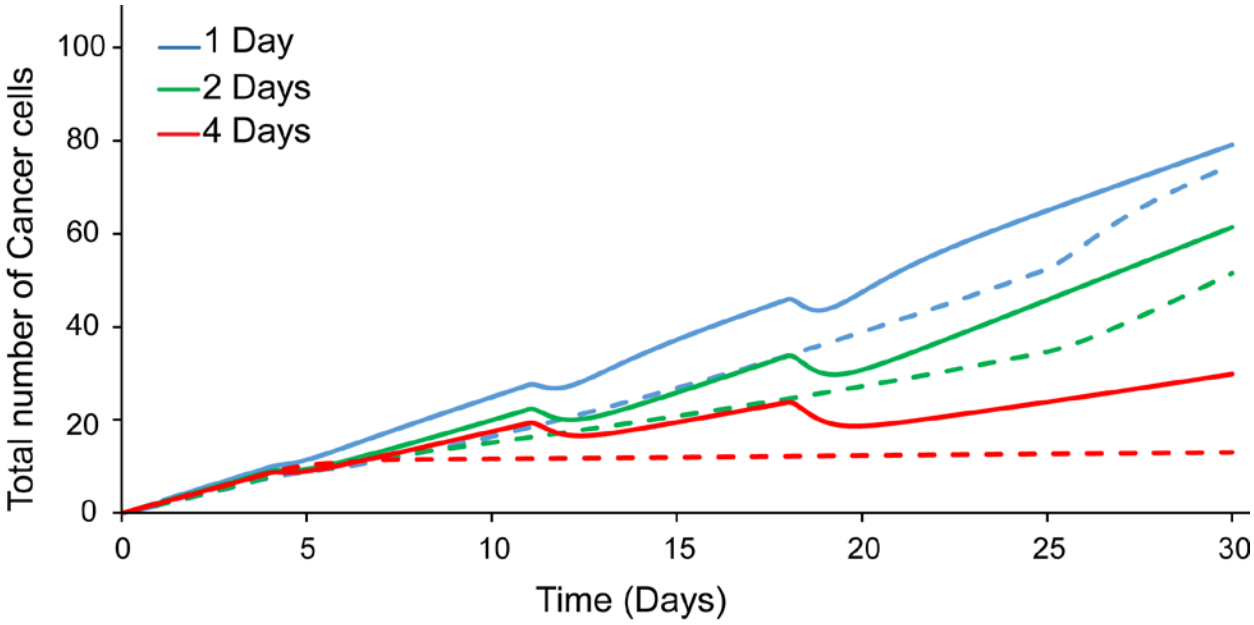

Figure S8 Comparison of model predictions with experimental data by Cham et. al. (35).

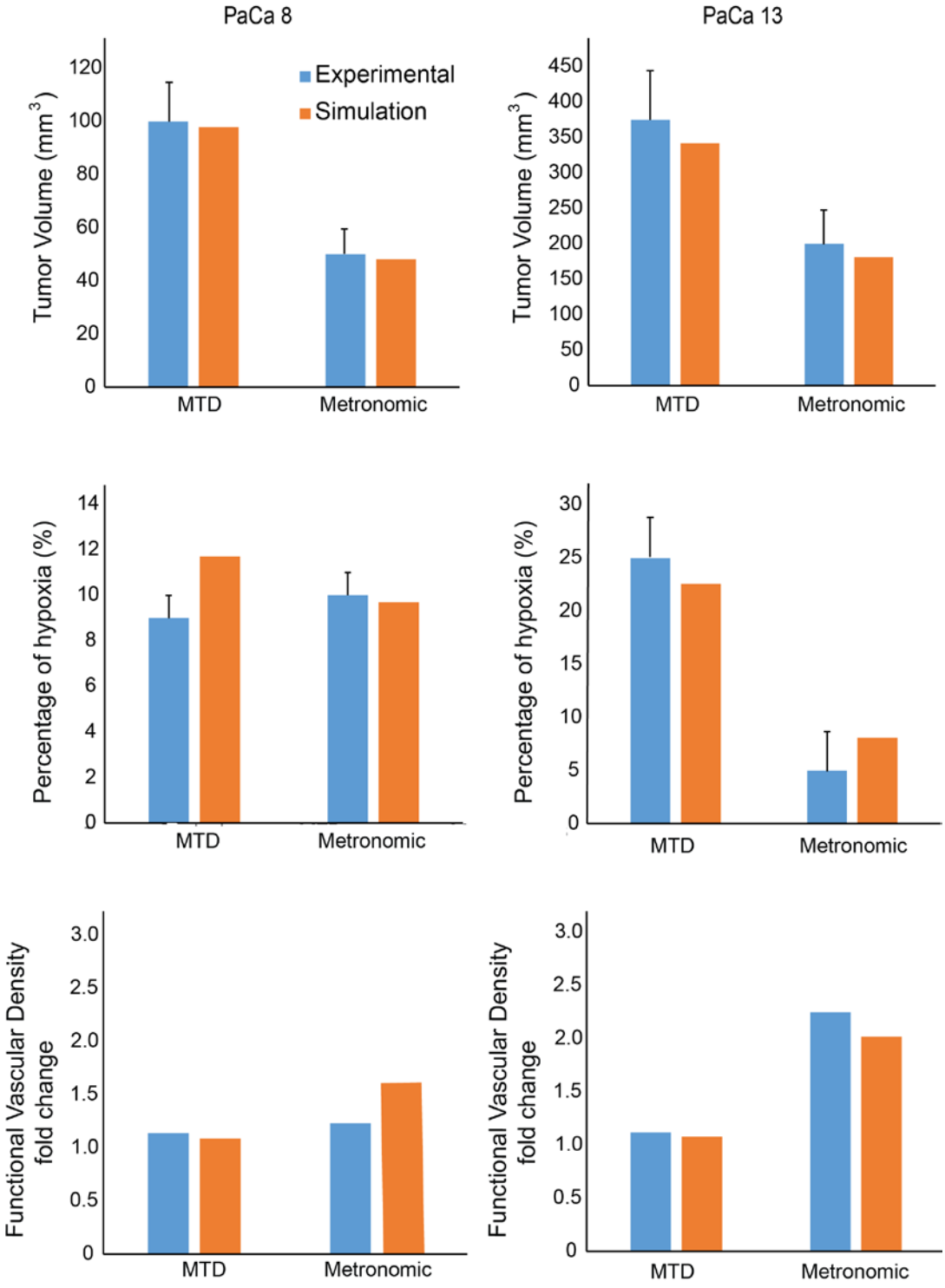

Figure S9 Comparison of model predictions with experimental data by Yapp. et. al. (46)

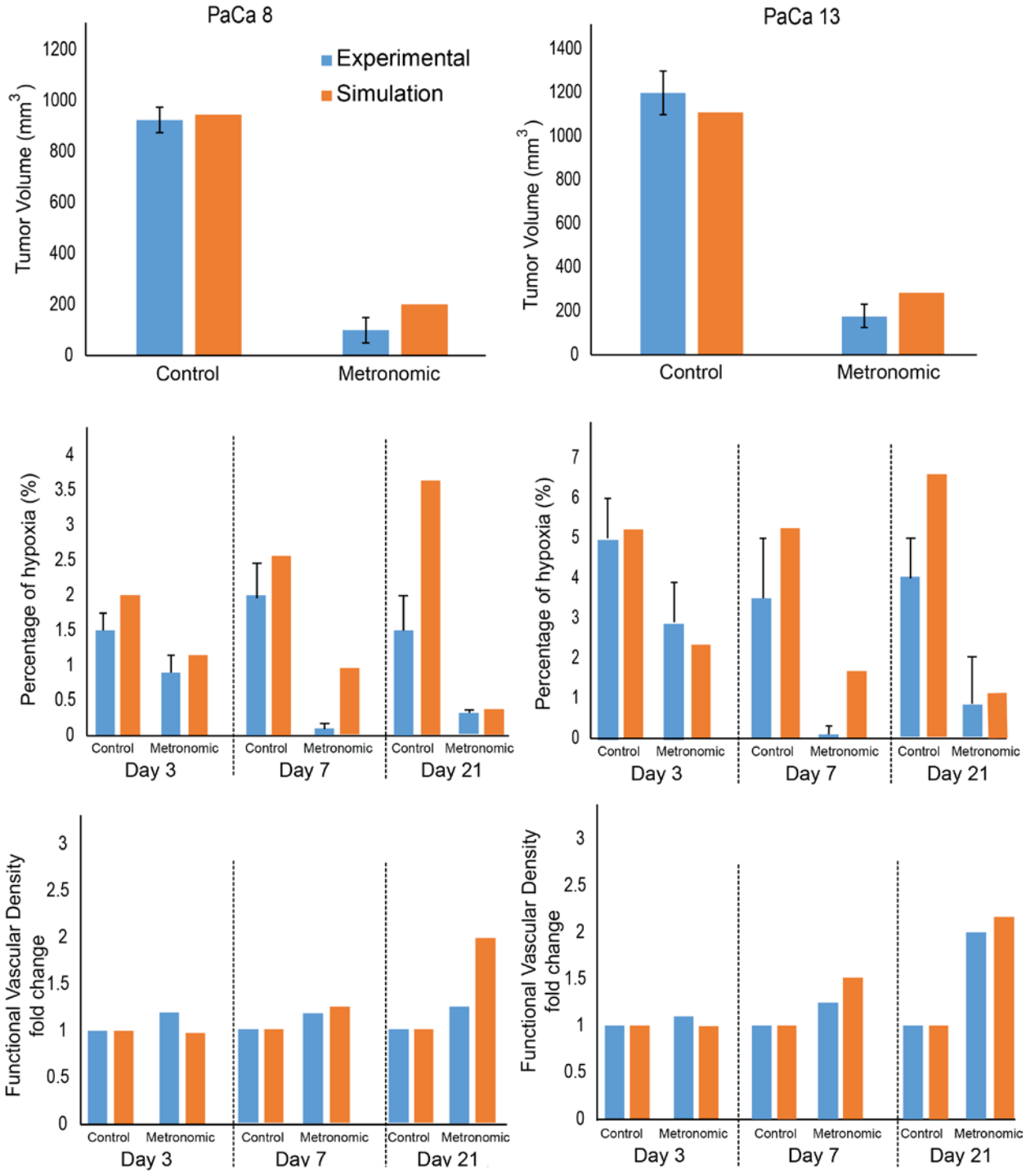

Figure S10 Internalized drug concentration as a function of the functional vascular density and the pore size (permeability) of the tumor vessel wall. Drug delivery is optimized for high vascular densities and for pore sizes on the order of 150 nm. Drug concentration is normalized by division with the concentration at the vessels.

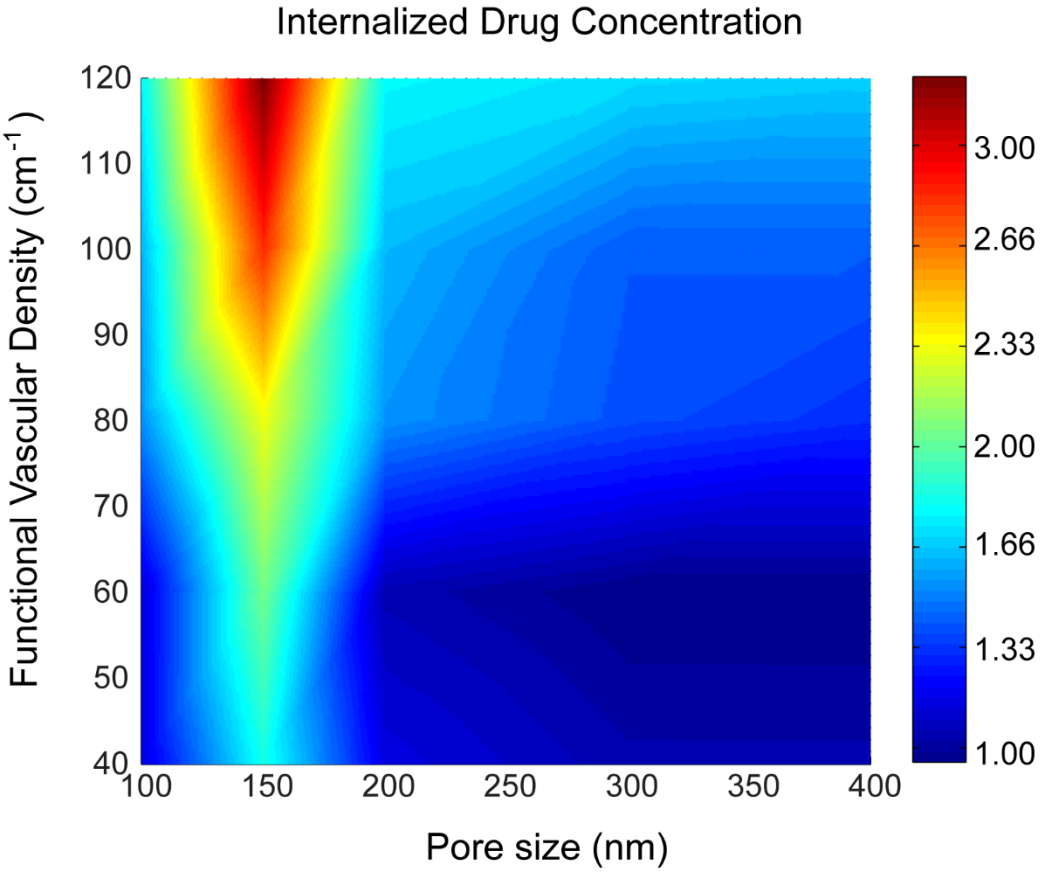

Figure S11 Model predictions of tumor growth with and without the effect of vascular normalization on immune response activation (A). The killing rates of NK (parameter c) and CD8+ T-cells (parameter d) have the baseline values and remain unaltered after normalization of tumor vessels. The results show that when immune activation in not accounted for metronomic therapy is still more effective compared to MTD, which is simply an effect of improved drug delivery. Predictions for two different times of tumor relapse are presented: (B) 3 days and (C) 5 days. The 1/14 dose schedule (compared to MTD) of metronomic therapy was employed.

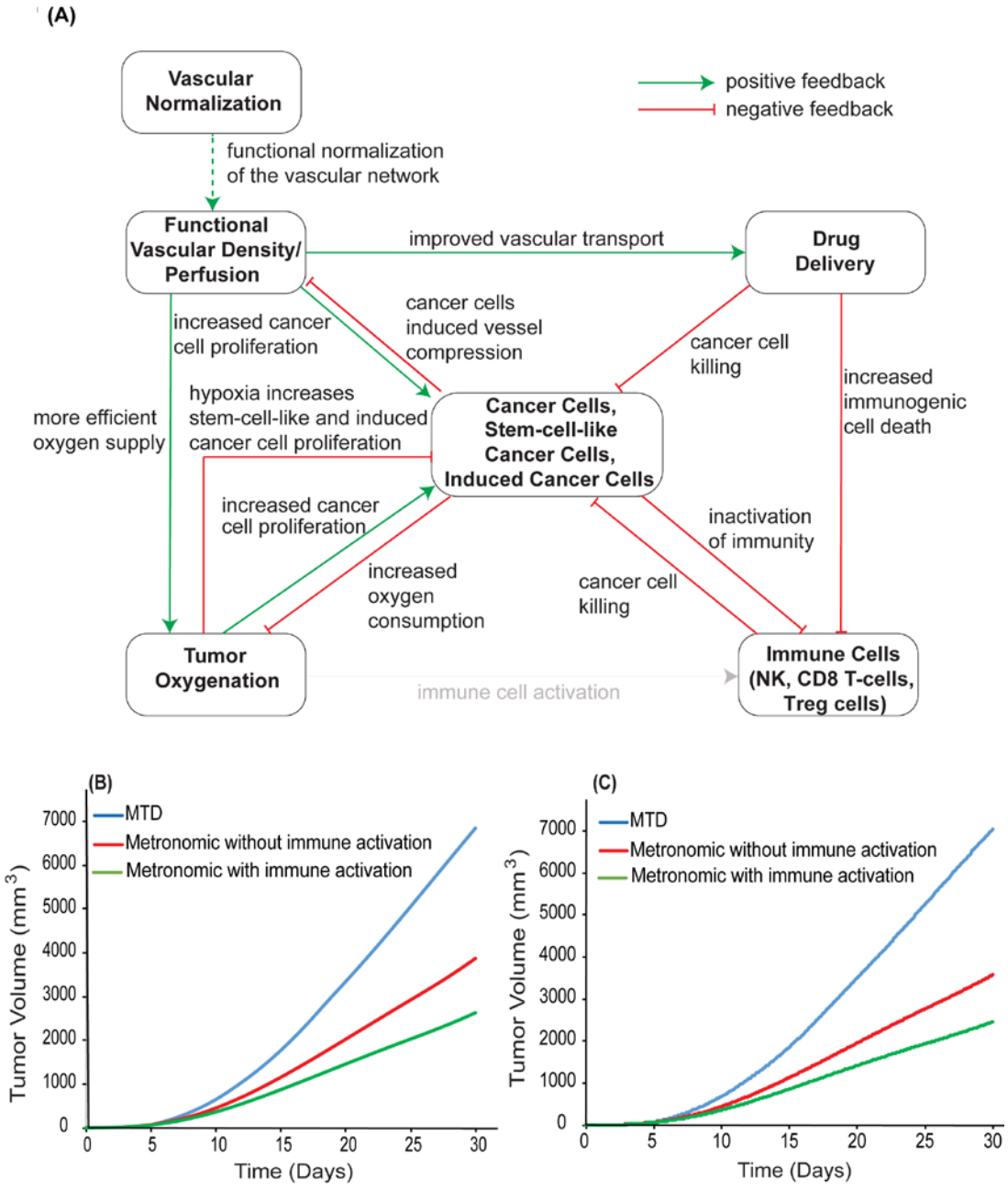

Figure S12 Model predictions of tumor growth when metronomic chemotherapy accounts only for immunogenic cell death and not changes in the tumor vasculature (A). Metronomic therapy reduces immunogenic cell death and results in smaller tumor volumes compared to MTD (B). The 1/14 dose schedule (compared to MTD) of metronomic therapy was employed.

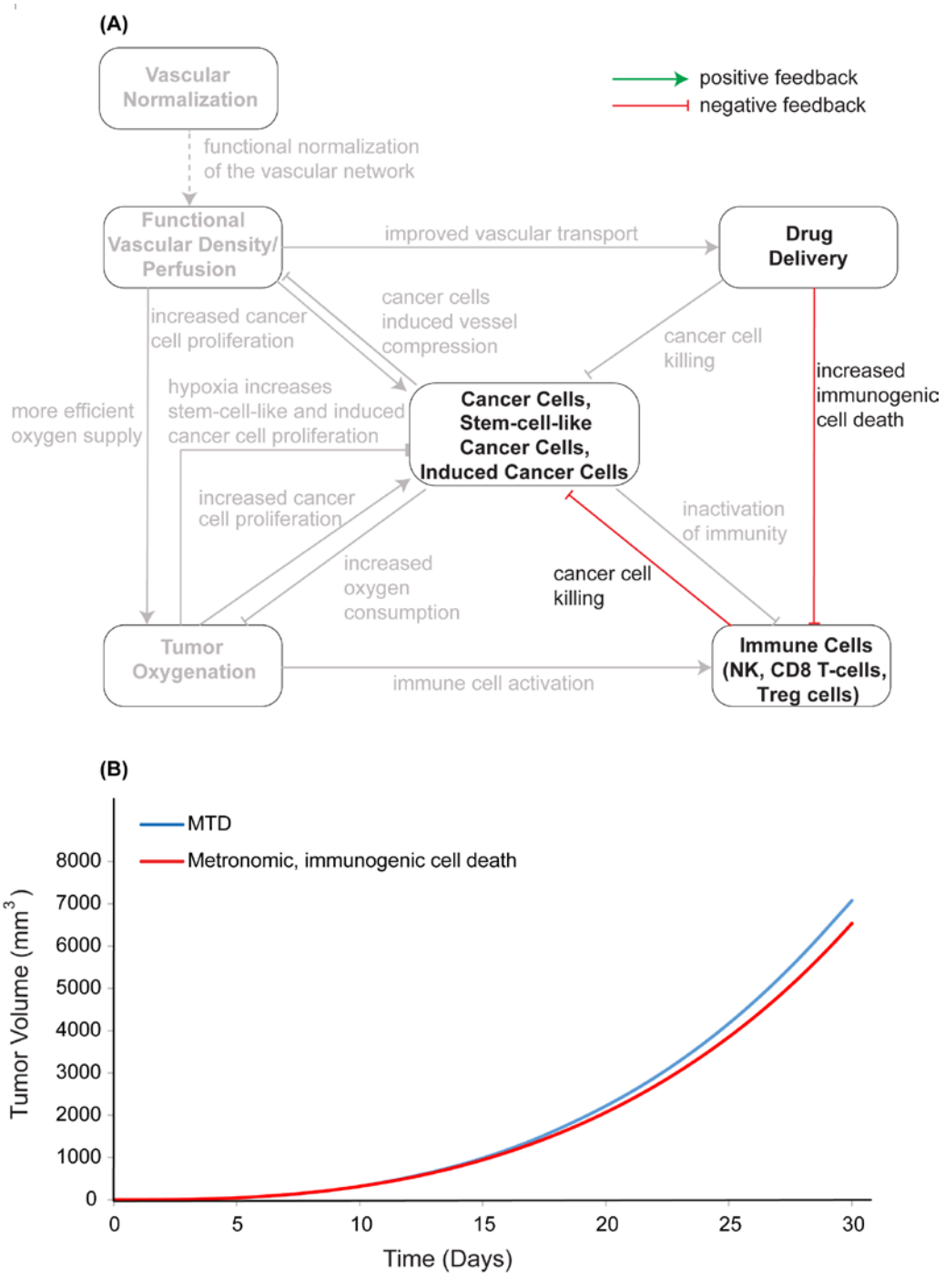

Figure S13 Model predictions of tumor growth as a function of the inhibition of immune cell activity by regulatory T cells. The corresponding parameter λ_{reg} in Eq. (5) was varied to receive a minimum (one order of magnitude lower) and a maximum (one order of magnitude higher) value from the baseline reported in Table S1. Increasing the value of λ_{reg} leads to higher tumor volumes because inhibition of immune response increases the density of cancer cells and cancer stem cells. The MTD protocol was employed for the simulations.

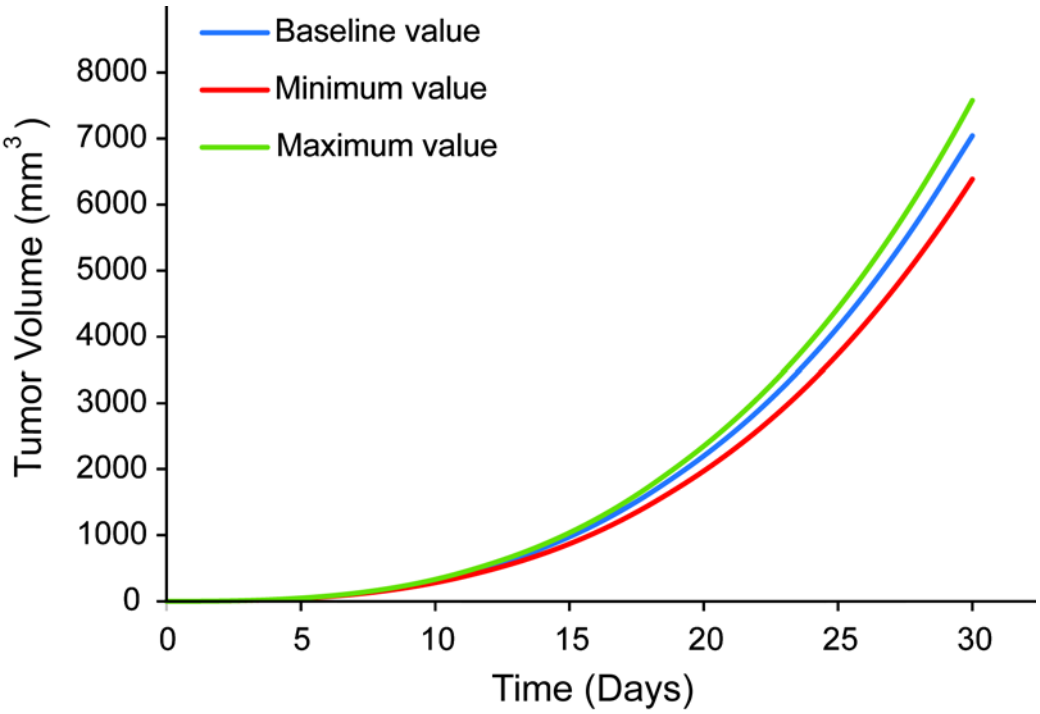

Figure S14 Dependence of vessel diameter on cancer cell density derived from the analysis of experimental data (28, 30). In the model cancer cell density is evaluated as the total number of cancer cells in the tumor (i.e., sum of cancer cells at each computational node) per unit area calculated as πr^2, where r is the tumor radius.

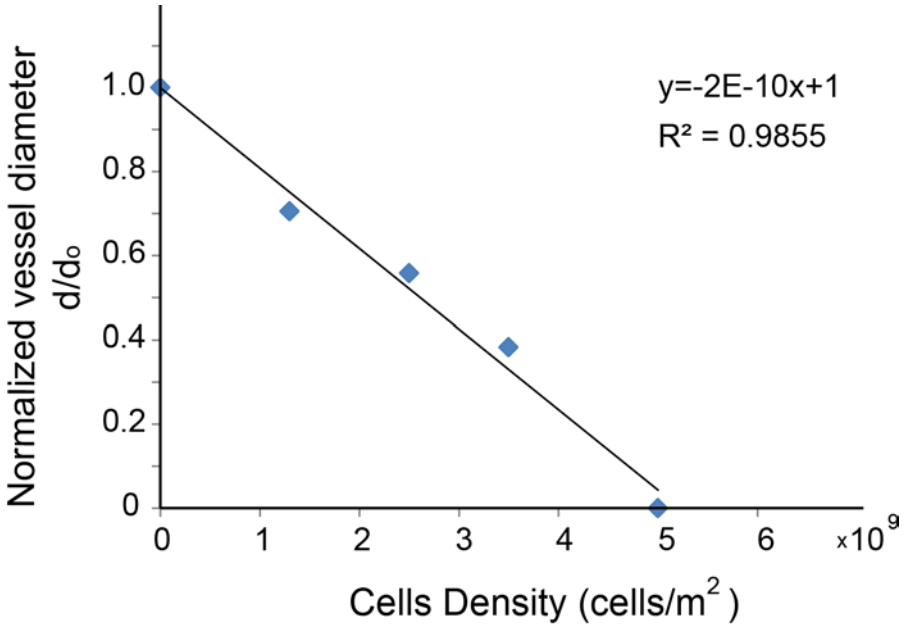

Figure S15 Computational domain and boundary conditions employed.

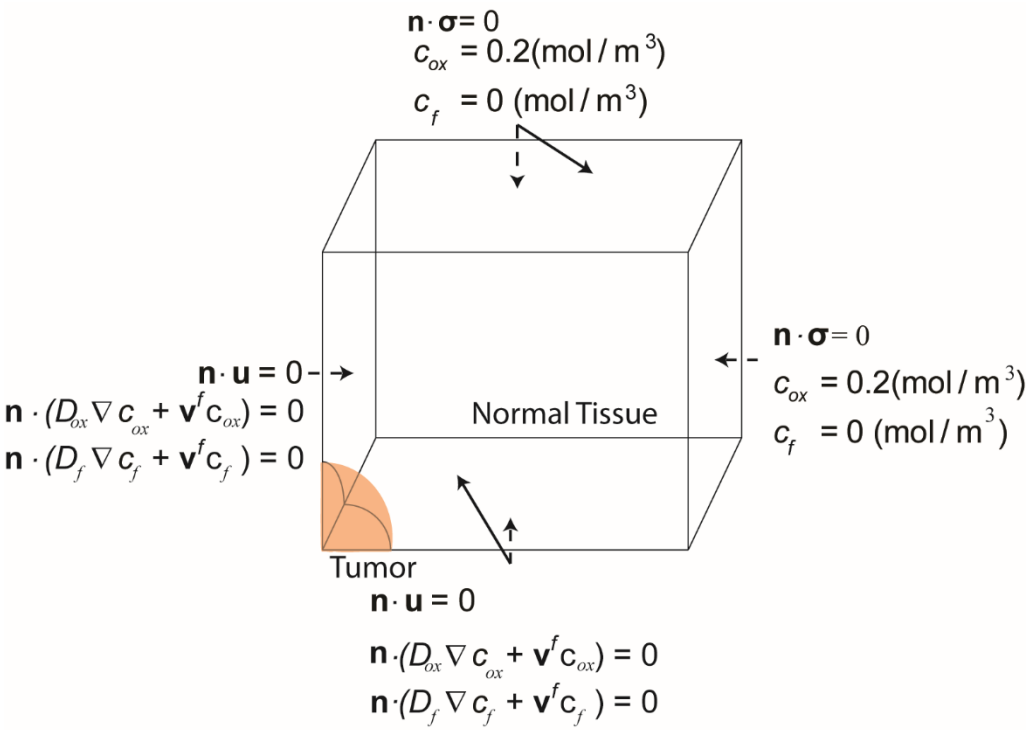

References

1. Rodriguez EK, Hoger A, & McCulloch AD (1994) Stress-dependent finite growth in soft elastic tissues. *Journal of biomechanics* 27(4):455-467.
2. Skalak R, Zargaryan S, Jain RK, Netti PA, & Hoger A (1996) Compatibility and the genesis of residual stress by volumetric growth. *Journal of mathematical biology* 34(8):889-914.
3. Roose T, Netti PA, Munn LL, Boucher Y, & Jain RK (2003) Solid stress generated by spheroid growth estimated using a linear poroelasticity model. *Microvasc Res* 66(3):204-212.
4. Kim Y, Stolarska MA, & Othmer HG (2011) The role of the microenvironment in tumor growth and invasion. *Prog Biophys Mol Bio* 106(2):353-379.
5. Stylianopoulos T*, et al.* (2013) Coevolution of solid stress and interstitial fluid pressure in tumors during progression: implications for vascular collapse. *Cancer research* 73(13):3833-3841.
6. MacLaurin J, Chapman J, Jones GW, & Roose T (2012) The buckling of capillaries in solid tumours. *P Roy Soc a-Math Phy* 468(2148):4123-4145.
7. Voutouri C & Stylianopoulos T (2014) Evolution of osmotic pressure in solid tumors. *J Biomech*.
8. Goldman A*, et al.* (2015) Temporally sequenced anticancer drugs overcome adaptive resistance by targeting a vulnerable chemotherapy-induced phenotypic transition. *Nature communications* 6:6139.
9. de Pillis LG, Radunskaya AE, & Wiseman CL (2005) A validated mathematical model of cell-mediated immune response to tumor growth. *Cancer research* 65(17):7950-7958.
10. Fouchet D & Regoes R (2008) A population dynamics analysis of the interaction between adaptive regulatory T cells and antigen presenting cells. *PloS one* 3(5):e2306.
11. Burroughs NJ, Oliveira BMPM, Pinto AA, & Ferreira M (2011) Immune response dynamics. *Math Comput Model* 53(7-8):1410-1419.
12. Conley SJ*, et al.* (2012) Antiangiogenic agents increase breast cancer stem cells via the generation of tumor hypoxia. *Proceedings of the National Academy of Sciences of the United States of America* 109(8):2784-2789.
13. Barsoum IB, Smallwood CA, Siemens DR, & Graham CH (2014) A mechanism of hypoxia-mediated escape from adaptive immunity in cancer cells. *Cancer research* 74(3):665-674.
14. Ghiringhelli F*, et al.* (2007) Metronomic cyclophosphamide regimen selectively depletes CD4(+) CD25(+) regulatory T cells and restores T and NK effector functions in end stage cancer patients. *Cancer Immunology Immunotherapy* 56(5):641-648.
15. Hermann PC*, et al.* (2007) Distinct populations of cancer stem cells determine tumor growth and metastatic activity in human pancreatic cancer. *Cell stem cell* 1(3):313-323.
16. Casciari JJ, Sotirchos SV, & Sutherland RM (1992b) Mathematical-Modeling of Microenvironment and Growth in Emt6/Ro Multicellular Tumor Spheroids. *Cell Proliferat* 25(1):1-22.
17. Casciari JJ, Sotirchos SV, & Sutherland RM (1992a) Variations in Tumor-Cell Growth-Rates and Metabolism with Oxygen Concentration, Glucose-Concentration, and Extracellular Ph. *J Cell Physiol* 151(2):386-394.
18. Kerr DJ, Kerr AM, Freshney RI, & Kaye SB (1986) Comparative Intracellular Uptake of Adriamycin and 4'-Deoxydoxorubicin by Non-Small Cell Lung-Tumor Cells in Culture and Its Relationship to Cell-Survival. *Biochem Pharmacol* 35(16):2817-2823.
19. Eikenberry S (2009) A tumor cord model for Doxorubicin delivery and dose optimization in solid tumors. *Theor Biol Med Model* 6.
20. Liu G*, et al.* (2006) Analysis of gene expression and chemoresistance of CD133+ cancer stem cells in glioblastoma. *Molecular cancer* 5:67.

21. Todaro M*, et al.* (2009) Efficient killing of human colon cancer stem cells by gammadelta T lymphocytes. *Journal of immunology* 182(11):7287-7296.
22. Mow VC, Kuei SC, Lai WM, & Armstrong CG (1980) Biphasic Creep and Stress-Relaxation of Articular-Cartilage in Compression - Theory and Experiments. *J Biomech Eng-T Asme* 102(1):73-84.
23. Taber LA (2008) Theoretical study of Beloussov's hyper-restoration hypothesis for mechanical regulation of morphogenesis. *Biomechanics and modeling in mechanobiology* 7(6):427-441.
24. Ciarletta P (2013) Buckling Instability in Growing Tumor Spheroids. *Phys Rev Lett* 110(15).
25. Voutouri C, Mpekris F, Papageorgis P, Odysseos AD, & Stylianopoulos T (2014) Role of constitutive behavior and tumor-host mechanical interactions in the state of stress and growth of solid tumors. *PloS one* 9(8):e104717.
26. Xu G, Bayly PV, & Taber LA (2009) Residual stress in the adult mouse brain. *Biomechanics and modeling in mechanobiology* 8(4):253-262.
27. Xu G*, et al.* (2010) Opening angles and material properties of the early embryonic chick brain. *Journal of biomechanical engineering* 132(1):011005.
28. Griffon-Etienne G, Boucher Y, Brekken C, Suit HD, & Jain RK (1999) Taxane-induced apoptosis decompresses blood vessels and lowers interstitial fluid pressure in solid tumors: clinical implications. *Cancer research* 59(15):3776-3782.
29. Stylianopoulos T & Jain RK (2013) Combining two strategies to improve perfusion and drug delivery in solid tumors. *Proceedings of the National Academy of Sciences of the United States of America* 110((46)):18632-18637.
30. Padera TP*, et al.* (2004) Pathology: cancer cells compress intratumour vessels. *Nature* 427(6976):695.
31. Olive KP*, et al.* (2009) Inhibition of Hedgehog signaling enhances delivery of chemotherapy in a mouse model of pancreatic cancer. *Science* 324(5933):1457-1461.
32. Stylianopoulos T & Jain RK (2013) Combining two strategies to improve perfusion and drug delivery in solid tumors. *P Natl Acad Sci USA* 110(46):18632-18637.
33. Deen WM (1987) Hindered Transport of Large Molecules in Liquid-Filled Pores. *Aiche J* 33(9):1409-1425.
34. Browder T*, et al.* (2000) Antiangiogenic scheduling of chemotherapy improves efficacy against experimental drug-resistant cancer. *Cancer research* 60(7):1878-1886.
35. Cham KK*, et al.* (2010) Metronomic gemcitabine suppresses tumour growth, improves perfusion, and reduces hypoxia in human pancreatic ductal adenocarcinoma. *British journal of cancer* 103(1):52-60.
36. Mupparaju S*, et al.* (2011) Repeated tumor oximetry to identify therapeutic window during metronomic cyclophosphamide treatment of 9L gliomas. *Oncology reports* 26(1):281-286.
37. Eder M*, et al.* (2014) Comparison of Different Material Models to Simulate 3-D Breast Deformations Using Finite Element Analysis. *Ann Biomed Eng* 42(4):843-857.
38. Samani A, Zubovits J, & Plewes D (2007) Elastic moduli of normal and pathological human breast tissues: an inversion-technique-based investigation of 169 samples. *Phys Med Biol* 52(6):1565-1576.
39. Netti PA, Berk DA, Swartz MA, Grodzinsky AJ, & Jain RK (2000) Role of extracellular matrix assembly in interstitial transport in solid tumors. *Cancer Res* 60(9):2497-2503.
40. Mok W, Stylianopoulos T, Boucher Y, & Jain RK (2009) Mathematical modeling of herpes simplex virus distribution in solid tumors: implications for cancer gene therapy. *Clinical cancer research : an official journal of the American Association for Cancer Research* 15(7):2352-2360.
41. Schmidt MM & Wittrup KD (2009) A modeling analysis of the effects of molecular size and binding affinity on tumor targeting. *Molecular cancer therapeutics* 8(10):2861-2871.

42. Pluen A*, et al.* (2001) Role of tumor-host interactions in interstitial diffusion of macromolecules: cranial vs. subcutaneous tumors. *Proceedings of the National Academy of Sciences of the United States of America* 98(8):4628-4633.
43. Chauhan VP*, et al.* (2012) Normalization of tumour blood vessels improves the delivery of nanomedicines in a size-dependent manner. *Nature nanotechnology* 7(6):383-388.
44. de Pillis LG, Radunskaya AE, & Wiseman CL (2005) A validated mathematical model of cell-mediated immune response to tumor growth. *Cancer research* 65(17):7950-7958.
45. Doloff JC*, et al.* (2009) Increased Tumor Oxygenation and Drug Uptake During Anti-Angiogenic Weekly Low Dose Cyclophosphamide Enhances the Anti-Tumor Effect of Weekly Tirapazamine. *Current Cancer Drug Targets* 9(6):777-788.
46. Yapp DT*, et al.* (2016) The differential effects of metronomic gemcitabine and antiangiogenic treatment in patient-derived xenografts of pancreatic cancer: treatment effects on metabolism, vascular function, cell proliferation, and tumor growth. *Angiogenesis* 19(2):229-244.
47. Izumi Y, Xu L, di Tomaso E, Fukumura D, & Jain RK (2002) Tumour biology: herceptin acts as an anti-angiogenic cocktail. *Nature* 416(6878):279-280.